



RESEARCH ARTICLE

10.1002/2017JD027326

Key Points:

- Countering climate responses result in low-temperature change relative to the large instantaneous radiative forcing that the BC perturbation causes
- Regionally, BC can have considerable impact on precipitation
- The intermodel spread is in general large, and 2.5 times higher if emissions instead of fixed BC concentrations are used in the simulations

Supporting Information:

- Supporting Information S1

Correspondence to:

C. W. Stjern,
camilla.stjern@cicero.oslo.no

Citation:

Stjern, C. W., Samset, B. H., Myhre, G., Forster, P. M., Hodnebrog, Ø. Andrews, T., ... Voulgarakis, A. (2017). Rapid adjustments cause weak surface temperature response to increased black carbon concentrations. *Journal of Geophysical Research: Atmospheres*, 122, 11,462–11,481. <https://doi.org/10.1002/2017JD027326>

Received 20 JUN 2017

Accepted 21 SEP 2017

Accepted article online 10 OCT 2017

Published online 6 NOV 2017

©2017. The Authors.

This is an open access article under the terms of the Creative Commons Attribution License, which permits use, distribution and reproduction in any medium, provided the original work is properly cited.

Rapid Adjustments Cause Weak Surface Temperature Response to Increased Black Carbon Concentrations

Camilla Weum Stjern¹ , Bjørn Hallvard Samset¹ , Gunnar Myhre¹ , Piers M. Forster² , Øivind Hodnebrog¹ , Timothy Andrews³ , Olivier Boucher⁴ , Gregory Faluvegi^{5,6} , Trond Iversen⁷ , Matthew Kasoar⁸ , Viatcheslav Kharin⁹ , Alf Kirkevåg⁷ , Jean-François Lamarque¹⁰ , Dirk Olivié⁷, Thomas Richardson², Dilshad Shawkí⁸ , Drew Shindell¹¹ , Christopher J. Smith² , Toshihiko Takemura¹² , and Apostolos Voulgarakis⁸

¹CICERO Center for International Climate and Environmental Research, Oslo, Norway, ²School of Earth and Environment, University of Leeds, Leeds, UK, ³Met Office Hadley Centre, Exeter, UK, ⁴Institut Pierre-Simon Laplace, Université Pierre et Marie Curie/CNRS, Paris, France, ⁵Center for Climate Systems Research, Columbia University, New York, NY, USA, ⁶NASA Goddard Institute for Space Studies, New York, NY, USA, ⁷Norwegian Meteorological Institute, Oslo, Norway, ⁸Department of Physics, Imperial College London, London, UK, ⁹Canadian Centre for Climate Modelling and Analysis, Victoria, British Columbia, Canada, ¹⁰NCAR/UCAR, Boulder, CO, USA, ¹¹Earth and Ocean Sciences Division, Duke University, Durham, NC, USA, ¹²Climate Change Science Section, Kyushu University, Fukuoka, Japan

Abstract We investigate the climate response to increased concentrations of black carbon (BC), as part of the Precipitation Driver Response Model Intercomparison Project (PDRMIP). A tenfold increase in BC is simulated by nine global coupled-climate models, producing a model median effective radiative forcing of 0.82 (ranging from 0.41 to 2.91) W m⁻², and a warming of 0.67 (0.16 to 1.66) K globally and 1.24 (0.26 to 4.31) K in the Arctic. A strong positive instantaneous radiative forcing (median of 2.10 W m⁻² based on five of the models) is countered by negative rapid adjustments (−0.64 W m⁻² for the same five models), which dampen the total surface temperature signal. Unlike other drivers of climate change, the response of temperature and cloud profiles to the BC forcing is dominated by rapid adjustments. Low-level cloud amounts increase for all models, while higher-level clouds are diminished. The rapid temperature response is particularly strong above 400 hPa, where increased atmospheric stabilization and reduced cloud cover contrast the response pattern of the other drivers. In conclusion, we find that this substantial increase in BC concentrations does have considerable impacts on important aspects of the climate system. However, some of these effects tend to offset one another, leaving a relatively small median global warming of 0.47 K per W m⁻²—about 20% lower than the response to a doubling of CO₂. Translating the tenfold increase in BC to the present-day impact of anthropogenic BC (given the emissions used in this work) would leave a warming of merely 0.07 K.

1. Introduction

As a strong absorber of shortwave radiation, black carbon (BC) emitted to the atmosphere has an influence on global and regional climate (Bond et al., 2013). The impacts of BC aerosols span from aerosol-radiation interaction (direct aerosol effect), through influences on cloud microphysics (aerosol-cloud interactions or indirect aerosol effects), to rapid adjustments involving modification of atmospheric stability and humidity and consequent modification of clouds (semidirect effects). Quantifying the magnitude of these impacts is crucial to our ability to provide accurate estimates of future climate change. However, the climate impact of aerosols in general, and BC in particular, is still associated with significant uncertainty (Bond et al., 2013; Boucher et al., 2016, 2013; Myhre & Samset, 2015; Samset, Myhre, & Schulz, 2014).

In the most recent report from the Intergovernmental Panel on Climate Change, the direct radiative forcing (RF) from fossil fuel and biofuel emissions of BC is evaluated to be +0.4 (+0.05, 0.8) W m⁻² (Boucher et al., 2013). The large uncertainty range in this estimate can be linked to the fact that both model-based and observational studies disagree on several aspects of BC influence on climate. For instance, there is still no consensus on the value of globally averaged BC emissions, although more recent studies point to previous underestimation of this number (Bond et al., 2013; Cohen & Wang, 2014; Stohl et al., 2013). Vertical BC profiles have been shown to be poorly constrained (Samset, Myhre, Herber, et al., 2014; Schwarz et al., 2013; Wang et al., 2014), there are model discrepancies in the magnitude and importance of the coating-enhancement

of ambient BC absorption (Boucher et al., 2016; Gustafsson & Ramanathan, 2016; Peng et al., 2016) as well as in factors such as dry and wet removal efficiency (Mahmood et al., 2016), and the contribution from brown carbon is still uncertain (Liu et al., 2014). BC also influences climate through indirect effects (microphysical influence of BC aerosols on cloud droplets, Twomey, 1974) and semidirect effects (BC absorption influences the short-wave heating rate, influencing the vertical temperature profile and/or causing evaporation of cloud droplets, Ackerman et al., 2000). When estimating indirect and semidirect effects of BC, a multitude of chemical, physical, and dynamical processes are involved on the path from emission to climate influence. Model differences in parametrizations of these processes induce particularly large spread in indirect and semidirect BC forcings (Bond et al., 2013). For instance, the semidirect effect can have opposite signs depending on where the BC is located in relation to the altitude of the cloud layer (Koch & Del Genio, 2010). This means that intermodel variation in both BC and cloud fields will greatly influence estimates of this effect, as found, for instance, in Hodnebrog, Myhre, and Samset (2014). Indeed, estimates of effective radiative forcing (ERF) from aerosol-cloud interactions (ERF_{aci}) have been shown to be highly dependent on model cloud fields. Zelinka et al. (2014) analyzed aerosol experiments in nine CMIP5 models and found that more than 20% of the intermodel spread in ERF_{aci} was caused by model differences in baseline cloud amounts. Samset and Myhre (2015) found substantial interannual differences in semidirect RF in simulations using the CESM-CAM4 model, primarily due to differences in cloud fraction, and pointed to the importance of cloud field representation and location relative to BC for estimates of the semidirect effect. Likewise, Chen and Penner (2005) identify aerosol burden and cloud fraction to be the most important sources of model disagreement in estimates of indirect aerosol effects.

Attempts to isolate and quantify the impact of BC on global climate are not abundant in the literature. Mahajan et al. (2013) found in simulations with a global climate model (GCM) a global warming of 0.52 K for a tenfold increase of present-day concentrations, relative to a scenario with no BC. Jones, Haywood, and Boucher (2007) found a globally averaged warming of 0.28 K in HadGEM1 simulations where year 2000 BC emissions were compared to a control run with emissions for year 1860. In a model study by Jacobson (2010), all fossil fuel soot (including BC and primary organic matter) was removed, which caused a significant cooling of -0.3 to -0.5 K globally and up to -1.2 K above the Arctic Circle. Similarly, Baker et al. (2015) found that removing all present-day BC in four GCMs lead to an average global change of -0.044 K, with a model/ensemble range from -0.152 to 0.085 K. The model spread was particularly large in the Arctic. Single-model studies of BC responses in the Arctic have shown relatively large responses to BC perturbations: Sand, Berntsen, Kay et al. (2013) found, using the NorESM1 model, that a tenfold increase in BC concentrations in midlatitudes caused a significant surface warming of 1.1 K in the Arctic. For local increases in Arctic BC, however, the response was a surface cooling, as also found in Shindell and Faluvegi (2009).

Comparison of BC responses between studies is often complicated by the fact that multiple climate drivers are changed simultaneously. And even if pure BC-perturbation experiments exist, they often differ in their setups and size of BC change (e.g., Baker et al., 2015; Sand, Berntsen, Seland et al., 2013). In the Precipitation Driver and Response Model Intercomparison Project PDRMIP (Myhre, Forster et al., 2017), 10 global climate models performed coordinated experiments (both in fully coupled modes as well as with fixed sea surface temperatures) where the main goal was to study the precipitation response to five different climate drivers separately, namely, CO₂, CH₄, BC, the total solar irradiance (TSI), and SO₄. The availability of this BC experiment, involving a tenfold increase in anthropogenic BC and hereafter referred to as BCx10, facilitates the opportunity to compare isolated climate system responses to BC among models.

First results from the PDRMIP project (Myhre, Forster et al., 2017; Samset et al., 2016) show that among the five climate drivers, there is a clear tendency for BC to give the highest relative intermodel spread in most climate responses. Myhre, Forster, et al. (2017) and Samset et al. (2016) also identify BC as the driver that has the weakest globally averaged temperature response with respect to the forcing and that produces some of the strongest precipitation reductions despite the global mean temperature increase. In this paper we take a closer look at the BCx10 experiment. We aim to understand why the climate response to this substantial increase in BC apparently involves a rather modest influence on surface temperature and to identify the main causes of the large intermodel spread in the climate response to BC. In the next section we give a brief introduction to the models, model setups, and experiments used in the analyses. In section 3 we describe the model differences in BC distribution, as well as climate responses to the BC perturbation. Changes in temperature, precipitation, and radiative forcing are shown, in addition to vertical changes in clouds and

Table 1
BC Treatment in the Different Models

	Emissions			BC MAC (m ² g ⁻¹)	BC emission change (Tg/yr)	BC burden change (mg m ⁻²)	BC life-time (days)
	BASE	BCx10	BC mixed state				
<i>Concentration-driven models</i>							
CESM-CAM4	Mostly year 2000 (Lamarque et al., 2010), although some variation; see Myhre et al. (2013).		External	7.30			
GISS-E2-R			External	6.24			
HadGEM3			External	3.36	45.5	1.80	7.4
IPSL-CM5A			External	~6			
NorESM1			Internal and external	7.96			
<i>Emission-driven models</i>							
CanESM2 [E]	-	-	Internal	-	76.5	4.41	10.73
CESM-CAM5 [E]	Year 2005, Lamarque et al. (2010)	Year 2005 × 10	Internal	9.85	46.4	0.85	3.41
HadGEM2-ES [E]	Year 1860, Lamarque et al. (2010)	Year 2000 × 10	External	3.29	50.1	5.82	21.33
MIROC-SPRINTARS [E]	Year 2010, Janssens-Maenhout et al. (2015)	Year 2010 × 10	Internal and external	4.03	69.2	1.98	5.33

Note. "Concentration-driven models" refer to models that use (the same AeroCom-based) fixed BC concentrations in the BASE experiment, and the anthropogenic part of these concentrations multiplied by 10 in the BCx10 experiment. "Emission-driven models" refer to models that use individual emissions (given in the table) for the BASE experiment, and those emissions multiplied by 10 in the BCx10 experiment. An exception in the latter group is HadGEM2-ES [E], which uses year 1860 emissions in BASE but year 2000 emission times 10 for the BCx10 experiment. Information on emissions or mass absorption coefficient (MAC) was not available for CanESM2 [E]. MAC was calculated as the change in absorption optical depth at 550 nm divided by the BC burden change.

relative humidity. The results, as well as how they compare to previous findings, are discussed in section 4 and summarized in section 5.

2. Data and Experiments

In the PDRMIP project, 10 global climate models simulated a baseline experiment using year 2000 greenhouse gas and aerosol concentrations or emissions (hereafter BASE). Relative to BASE, each model then simulated five perturbation experiments: a doubling of CO₂ concentrations (hereafter CO₂x2), a tripling of CH₄ concentrations (CH₄x3), a 2% increase in the TSI (SOL), an increase in anthropogenic BC concentrations or emissions by a factor of 10 (BCx10), and an increase in anthropogenic SO₄ concentrations or emissions by a factor of 5 (SO₄x5). We refer back to Myhre, Forster et al. (2017) for a full description of model setups and experiments.

To limit the number of unintended sources of intermodel differences in the aerosol experiments, five of the models fixed their BASE BC (and SO₄) concentrations to the monthly multimodel mean present-day concentrations from AeroCom Phase II (Myhre et al., 2013; Samset et al., 2013) and simulated the BCx10 experiment using a tenfold increase in the anthropogenic portion of these concentrations. These AeroCom concentrations are primarily based on year 2000 Lamarque et al. (2010) emissions, as given in the upper part of Table 1. For the remaining models, however, the model design precluded the use of prescribed aerosol concentration fields as input. In these models, the BASE simulation was run using present-day BC emissions, while the BCx10 simulation was run with 10 times larger anthropogenic emission levels. This difference in simulation setup is not trivial, as will be shown later. The BC emissions used in the BASE simulation for the emission-driven models are given in the lower part of Table 1—note that HadGEM2 used year 1860 instead of present-day emissions as a baseline. One model (MPI-ESM) was not able to perform the aerosol simulations, which means that the BCx10 case was performed by the following nine models, where [E] denotes that the model used increased emission-driven BC instead of increased prescribed concentrations: CanESM2 [E], CESM-CAM4, CESM-CAM5 [E], GISS-E2-R, HadGEM2-ES [E], HadGEM3, IPSL-CM5A, NorESM1, and MIROC-SPRINTARS [E]. Note that although HadGEM2-ES [E] used preindustrial emissions in their BASE run, their BCx10 run was based on 10 times the anthropogenic emissions of year 2000, see Table 1.

All experiments were run in an atmosphere-only configuration where sea surface temperatures were prescribed (hereafter referred to as fSST) as well as in a fully coupled atmosphere-ocean configuration (coupled). The simulation lengths for these two configurations were 15 and 100 years, of which years 6–15 and 51–100 were used in the analyses, respectively. In the results, "change" refers to the difference between the BCx10 and the BASE simulation.

The methods in the literature used to diagnose radiative flux changes at the top-of-atmosphere (TOA) varies, each having its own advantages and disadvantages (see, e.g., Sherwood et al., 2015). We here follow the line of previous PDRMIP publications: effective radiative forcing (ERF) is calculated as the change in net radiative long-wave (LW) plus short-wave (SW) fluxes at TOA in the fSST simulations (see Forster et al., 2016, for a discussion of different ways to diagnose the ERF). Instantaneous radiative forcing (IRF), supplied by five of the models, was simulated through double radiation calls; see Ghan et al. (2012). The IRF is similar to the direct aerosol effect or R_{Fari} in the IPCC AR5 terminology (Boucher et al., 2013).

The ERF includes the rapid adjustments (often referred to as the fast responses). Rapid adjustments include changes to the vertical temperature profile and the atmospheric humidity, both of which may influence cloud fractions. The part of this change in cloud fraction that is directly caused by local BC warming in the vicinity of the cloud is often referred to as the semidirect effect (Koch & Del Genio, 2010). In addition, BC-induced rapid adjustments in cloud fractions and precipitation may occur as a consequence of solar dimming (the surface energy budget effect, see, e.g., Lohmann & Feichter, 2005), as a result of circulation changes (e.g., Kovilakam & Mahajan, 2016), or due to microphysical influence of BC aerosols in warm or cold clouds (the indirect aerosol effect, e.g., Zhuang et al., 2013). Here we calculate rapid adjustments as the change between perturbation simulation and BASE for the fSST runs. The feedback response (sometimes referred to as the slow response) was diagnosed as the difference between the coupled and the fSST runs.

3. Results

3.1. Black Carbon Distribution

The change in total BC burden for the BCx10 experiment is shown in Figure 1 (first row), averaged globally as well as over six different latitude bands. The geographical pattern of the BC change can be seen in Figure S1 in the supporting information for the average of all models, as well as averaged separately over models using concentration-driven setups and over models using emission-driven setups. The largest increases occur over Southeast Asia and central Africa, followed by South America, Europe, and North America. The globally averaged change in BC burden varies among the models, with CanESM2 [E] and HadGEM2-ES [E] showing the largest changes and CESM-CAM5 [E] showing the smallest change (Figure 2 and Table 1). Ideally, the differences in BC burden should be minor, but the use of emission-driven setups in some models (including the three just mentioned) results in BC distributions that differ considerably from the prescribed BC perturbation.

Figure 2 shows globally averaged profiles of BC for the BASE (dashed) and BCx10 (solid) cases in the left panel, and the difference between the two cases in the right panel, and reveals important model discrepancies. HadGEM2-ES [E] and CanESM2 [E], which used emission-driven setups, have low BASE concentrations (recall that HadGEM2-ES [E] used year 1860 emissions for the BASE runs), but higher concentrations for the BCx10 case than all other models at all vertical layers. MIROC-SPRINTARS [E], which also simulated BCx10 based on emissions, has high increases in BC at lower atmospheric levels but has the lowest increase in BC of all models above about 300 hPa. This illustrates one of the challenges in model intercomparison projects; differing experimental setups will hamper a clean and straightforward analysis.

3.2. Temperature Changes

The BCx10 (coupled) simulations produce a globally averaged model median warming of 0.67 (0.16 to 1.66) K, where the spread indicates the lowest and highest individual model values (Table 2). Assuming linearity, this corresponds to a present-day warming of 0.074 K due to anthropogenic BC, given the present-day BC emissions used in this work. Baker et al. (2015) performed an experiment where all anthropogenic (present-day) BC was removed in simulations with four climate models. This resulted in a model mean globally averaged cooling of -0.044 K, with an ensemble range of -0.152 to 0.085 K. Had our experiment been a BC reduction instead of an increase, translating it to a "BCx0" scenario would give a cooling of -0.067 K, well within the uncertainty range given by Baker et al. (2015). Examining the linearity of the climate response from BC, Mahajan et al. (2013) performed simulations with increasing BC perturbations using the CAM4 model. The many investigated aspects of climate change (e.g., the TOA forcing, global temperature, cloud cover, and precipitation) were found to change linearly as the BC burden was increased. Relative to a BCx0 scenario they found a global warming of 0.52 K for the BCx10 simulation.

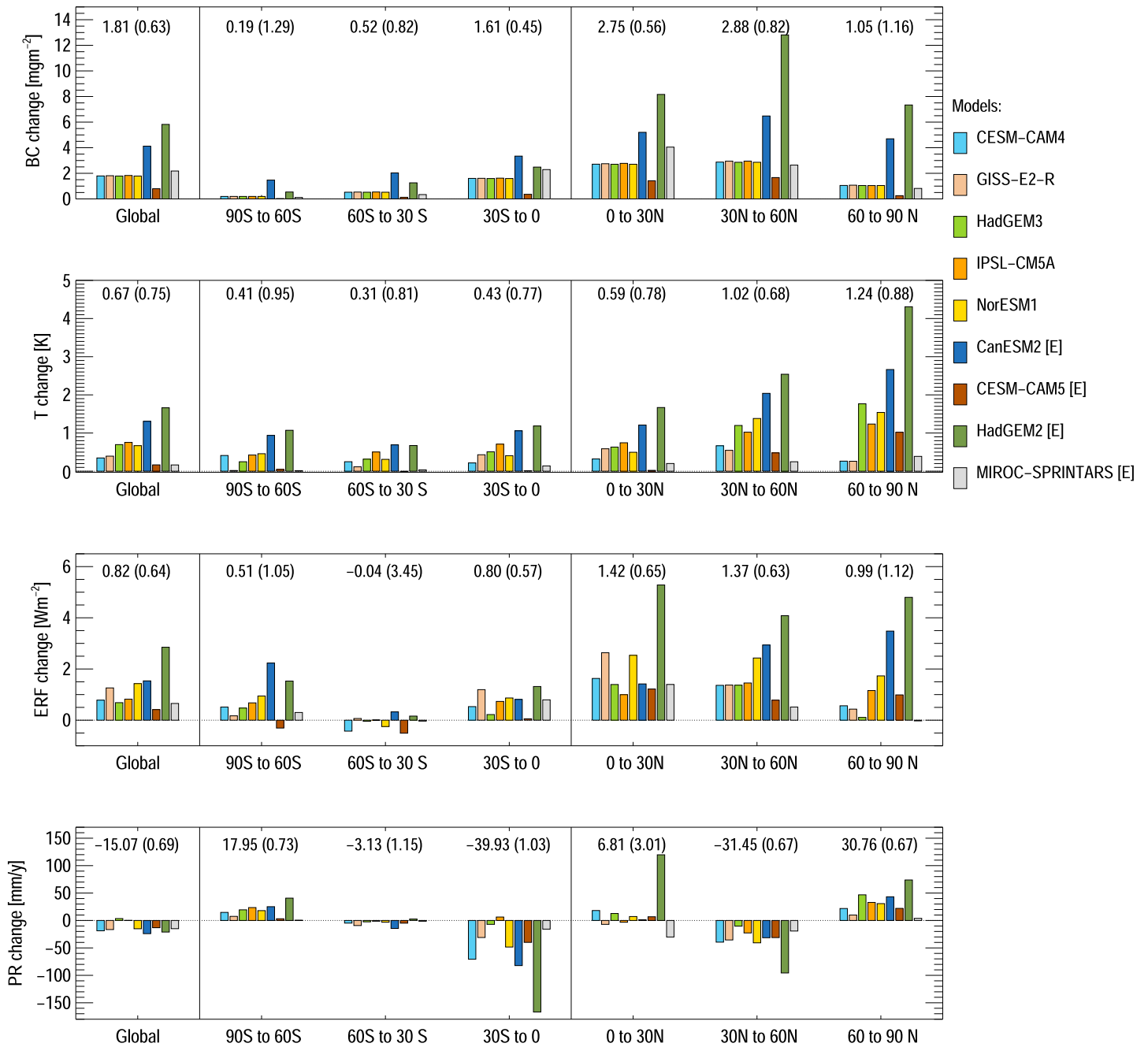


Figure 1. (first row) BCx10 minus BASE difference in BC load, (second row) near-surface temperature, (third row) ERF, and (fourth row) precipitation. Changes are based on years 51–100 of the coupled runs, except for ERF which is based on the years 6–15 of the fSST runs. The leftmost groups of bars show the global mean responses, while the remaining groups are averages over the latitude bands indicated on the x axis. Numbers above the groups of bars show region averages (relative intermodel standard deviation in parentheses) for the given latitude band.

As Figure 1 (second row) shows, the temperature change is largest in the Northern Hemisphere, which is expected as this is where most of the BC sources are located. The relative standard deviations (RSDs; given in parenthesis above the bars) are largest poleward of 60° in both hemispheres. The RSD of 0.75 for the global mean temperature change drops to 0.33 if we include only the models with concentration-driven simulations. Hence, a substantial part of the intermodel spread is caused by the fact that the BC perturbations are not the same for all models. The same can be seen from Figure S2, which shows a version of Figure 1 where the three lowest rows have been normalized by the change in BC load. The globally averaged

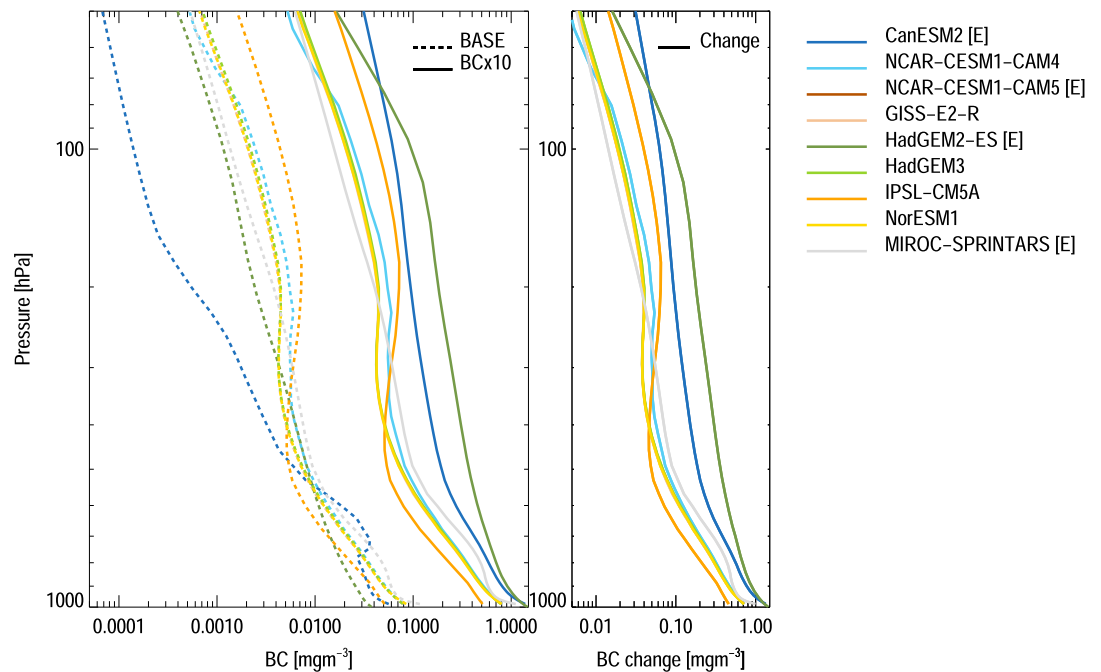


Figure 2. (left) Globally averaged profiles of black carbon for the BASE and BCx10 cases and the (right) difference between the two. Models that use emission-driven simulations instead of fixed concentrations are marked with [E]. Values for HadGEM3 and GISS-E2-R are almost identical to those of NorESM1 and are consequently mostly hidden behind the yellow line. CESM-CAM5 [E] was not able to provide the BC concentrations and is therefore not plotted.

BC-normalized temperature change has an RSD of 0.4, and the models with the largest normalized temperature changes are now IPSL-CM5A, HadGEM3, and NorESM1.

The Arctic warming amounts to 1.24 K, with a large intermodel range from 0.26 to 4.31 K. This is comparable to Sand, Berntsen, Kay et al. (2013), who studied the sensitivity of Arctic surface temperature to local and remote BC changes using the NorESM1 model and found that a tenfold increase in BC concentrations at mid-latitudes leads to a significant surface warming of 1.1 K in the Arctic. Note that NorESM1 includes the radiative effects of BC on snow and ice, as do also CESM-CAM5 [E] and MIROC-SPRINTARS [E] in the PDRMIP simulations. In NorESM1, which used prescribed BC concentrations here, the BC deposition was also enhanced by 10 in the simulations.

Table 2
Radiative Forcing and Temperature Values for the BCx10 Case

	ERF (W m ⁻²)	Norm. ERF (W g ⁻¹)	Temp. Change (K)	IRF (W m ⁻²)	Rapid adj. flux response (W m ⁻²)	Indir. aerosol effects from BC	Climate sensitivity (K (W m ⁻²) ⁻¹)	Efficacy
CanESM2 [E]	1.54	350	1.31	-	-	-	0.85	1.12
CESM-CAM4	0.78	430	0.35	2.10	-1.32	No	0.44	0.51
CESM-CAM5 [E]	0.41	490	0.17	-	-	No	0.04	0.06
GISS-E2-R	1.26	640	0.39	1.88	-0.64	No	0.31	0.86
HadGEM2-ES [E]	2.91	490	1.66	3.29	-0.39	No	0.58	0.73
HadGEM3	0.68	380	0.70	-	-	No	1.02	0.99
IPSL-CM5A	0.82	440	0.75	2.33	-1.44	Yes	0.92	1.21
NorESM1	1.43	750	0.67	-	-	Yes	0.47	0.80
MIROC-SPRINTARS [E]	0.65	330	0.16	1.22	-0.55	Yes	0.25	0.63
Median (±SD)	0.82 (±0.74)	490 (±150)	0.67 (±0.50)	2.10 (±0.76)	-0.64 (±0.48)	-	0.47 (±0.33)	0.80 (±0.35)

Note. IRF and rapid adj. flux response are only available for models that performed additional double call simulations. Normalized ERF is the ERF divided by the BC burden change. Dashed entries mean that the given information was not available for that model. Note that the climate sensitivity is here defined as the temperature change normalized by the ERF, both calculated from the difference between the BCx10 and the BASE simulation.

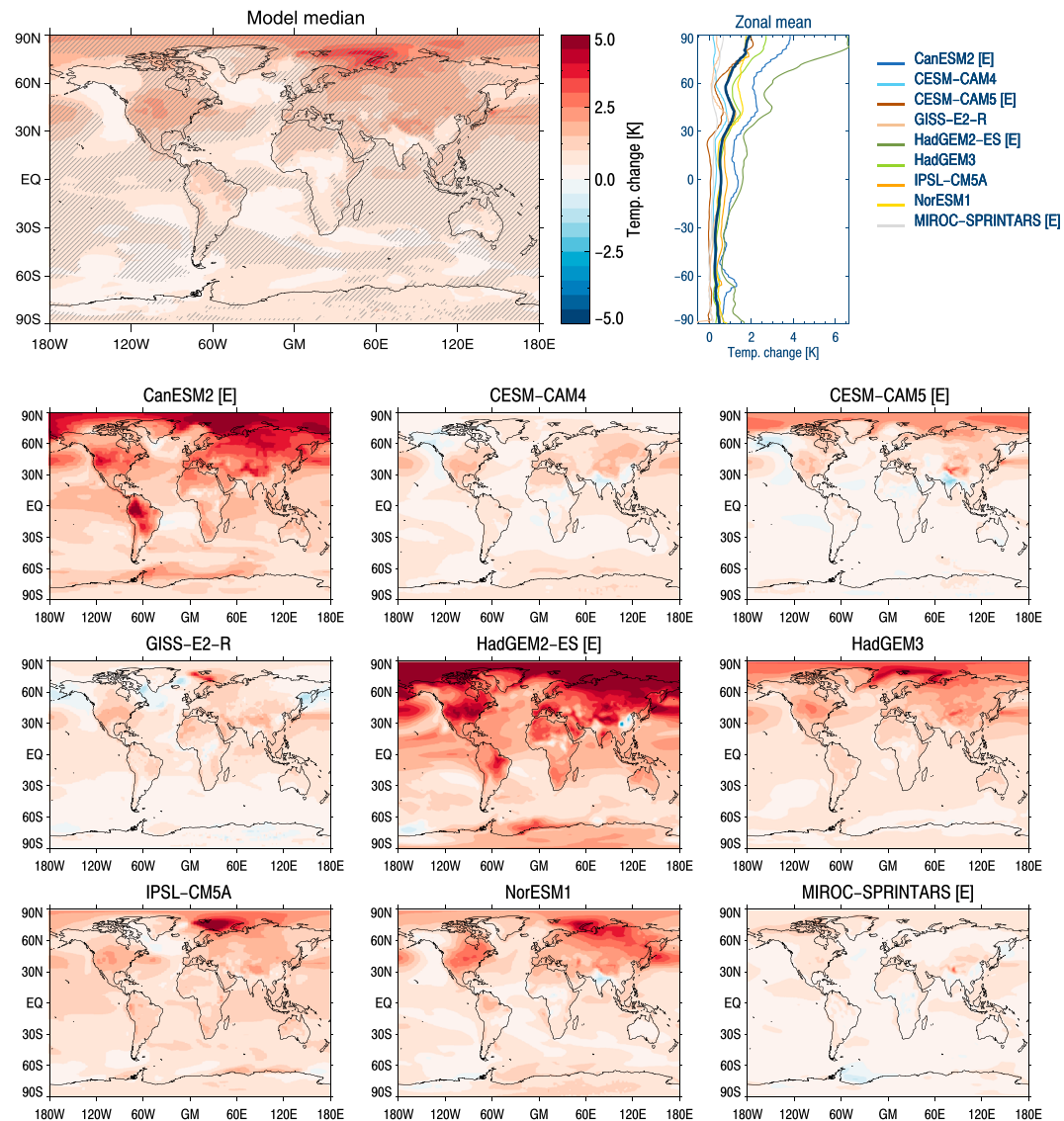


Figure 3. Annual mean model median change in near-surface temperature (top left), as well as zonally averaged temperature change for the model median (black line) and individual models (top right). The remaining panels show individual model results. Data are based on the last 50 years of the coupled runs, and hatched areas in the model median map indicate grid cells for which values are more than one multimodel standard deviation away from zero.

Figure 3 shows temperature change maps for the model median and individual models, as well as zonally averaged changes for each model, for the coupled runs. As seen in Figure 1, the temperature increase is largest on the Northern Hemisphere, where the BC concentrations change the most. However, at the “hot spots” of BC increase (India, China, and Central Africa; see Figure S1), the rapid temperature response is a significant cooling (not shown), caused by the strong reduction in surface heating as less shortwave radiation reaches the surface (solar dimming, see, e.g., Stanhill & Cohen, 2001). This initial cooling response reduces the total temperature response to only a weak warming (or for some models, a weak cooling) in these regions. All models but GISS-E2 R simulate an Arctic amplification (larger warming when averaged over the Arctic than when averaged globally); see Table S1.

3.3. Radiative Forcing

The ERF from BC_{x10}, estimated as the difference in TOA radiative flux in the fixed-SST runs, is 0.8 (0.4 to 2.9) W m⁻² globally, and 1.0 (−0.02 to 4.8) W m⁻² in the Arctic; see Figure 1. Here the highest model

values are from HadGEM2-ES [E] (2.9 and 4.8 W m^{-2} , respectively), while the next highest values are from CanESM2 [E] (1.5 and 3.5 W m^{-2} , respectively). Recall that the tenfold increase in BC investigated here is not a realistic scenario. Assuming linearity (see Hodnebrog et al., 2014, for a discussion of the impact of scaling and the linearity assumption on BC radiative forcing for the CESM-CAM4 model), the model medians translate into 1850–2000 BC forcings of 0.09 and 0.11 W m^{-2} (given the emissions used here) globally and in the Arctic, respectively. This is substantially lower than the combined direct and semidirect aerosol effect from Bond et al. (2013) and Boucher et al. (2013), but in line with various simulations in Hodnebrog et al. (2014). A main reason is likely the difference in emissions, which are about twice as high in Bond et al. (2013) as in Hodnebrog et al. (2014), and the compensating scaling of the semidirect effect in Hodnebrog et al. (2014) which is not present to the same degree in the analysis in Bond et al. (2013). In the present study, this compensation will be more explicitly treated as we use fully coupled, dynamical models.

Again, HadGEM2-ES [E] and CanESM2 [E] generally have values higher than the other models, and the global RSD of 0.64 drops to 0.33 when only the models with concentration-driven simulations are considered, or to 0.32 when normalizing ERF by the BC burden change (the second row in Figure S2). Normalized ERF is also given in Table 2. Note that for this quantity, the value for HadGEM2-ES [E] is equal to the model median, and for CanESM2 [E] it is even slightly below. Global maps of the ERF for individual models are given in Figure 4.

Table 2 shows the climate sensitivity of each model, defined here as the global temperature change divided by the ERF. The model median climate sensitivity for the BCx10 experiment amounts to $0.47 (0.04\text{--}1.02) \text{ K (W m}^{-2}\text{)}^{-1}$, which is about 20% lower than for the CO₂x2 experiments. The BC efficacy, calculated as the climate sensitivity for BCx10 divided by the climate sensitivity for CO₂x2, is 0.80 (0.06 to 1.21), where CESM-CAM5 [E] and IPSL-CM5A have the lowest and highest values, respectively.

Previous studies have shown that rapid adjustments play an important part in the climate impact of BC (Myhre, Forster et al., 2017; Samset et al., 2016). To get an idea of how much the rapid adjustments contribute to the total ERF, five of the models (MIROC-SPRINTARS [E], CESM-CAM4, HadGEM2-ES [E], GISS-E2-R, and IPSL-CM5A) performed double call runs to extract the IRF from BCx10. The model median IRF amounted to 2.10 W m^{-2} ; see Table 2. The rapid adjustment may then be estimated as the difference between a model's ERF and IRF. Depending on the model formulations, this rapid adjustment can comprise changes to both temperature, water vapor, and clouds and also microphysical effects of BC on clouds. As listed in Table 2, HadGEM2-ES [E], GISS-E2-R, and CESM-CAM4 do not include indirect effects from BC, which means that the rapid adjustments producing the difference between ERF and IRF come mainly from changes to clouds, temperature, and water vapor. A minor contribution could also come from changes in surface albedo over land. For MIROC-SPRINTARS [E] and IPSL-CM5A, there will be an additional contribution from the indirect effect within this estimate. As accounted for by Takemura et al. (2005), the microphysical effect of BC on warm clouds is very small in MIROC-SPRINTARS [E], but the contribution from BC on ice clouds can be of importance (Takemura et al., 2009). Additional simulations with IPSL-CM5A allowed for quantification of the IRF from aerosol-cloud interactions ("IRFaci") for this model, as seen in Figure S3. The global average of this effect was -0.07 W m^{-2} . Note that as the indirect RF was available for IPSL-CM5A, the rapid adjustment flux response was calculated as $\text{ERF} - \text{IRF} - \text{IRFaci}$ (as opposed to just $\text{ERF} - \text{IRF}$ for the other models).

As given in Table 2, the model median rapid adjustment flux response amounts to -0.64 W m^{-2} , with individual values ranging from -0.39 W m^{-2} (HadGEM2-ES [E]) to -1.44 W m^{-2} (IPSL-CM5A). For HadGEM2-ES [E], the value is about 10% the magnitude of the IRF, for GISS-E2-R and MIROC-SPRINTARS [E] it is around 30%, while for CESM-CAM4 and IPSL-CM5A it is around 60%. While generally weaker than the IRF, the rapid adjustment flux response does in some regions outweigh it; see Figure 5. For instance, in the tropical/subtropical North and South Atlantic (except close to the equator), a negative flux change from the rapid adjustments more than cancels the positive IRF, producing a negative total ERF (Figure 4). For GISS-E2-R a strong negative rapid adjustment signal in northern midlatitude ocean regions (particularly in the Pacific) is strong enough to produce a surface cooling (Figure 3).

3.4. Vertical Distribution of Changes

In Figure 6 we show globally averaged changes in the vertical profiles of temperature, cloud amount, and relative humidity, based on the coupled simulations. For BCx10, most models show an increase in

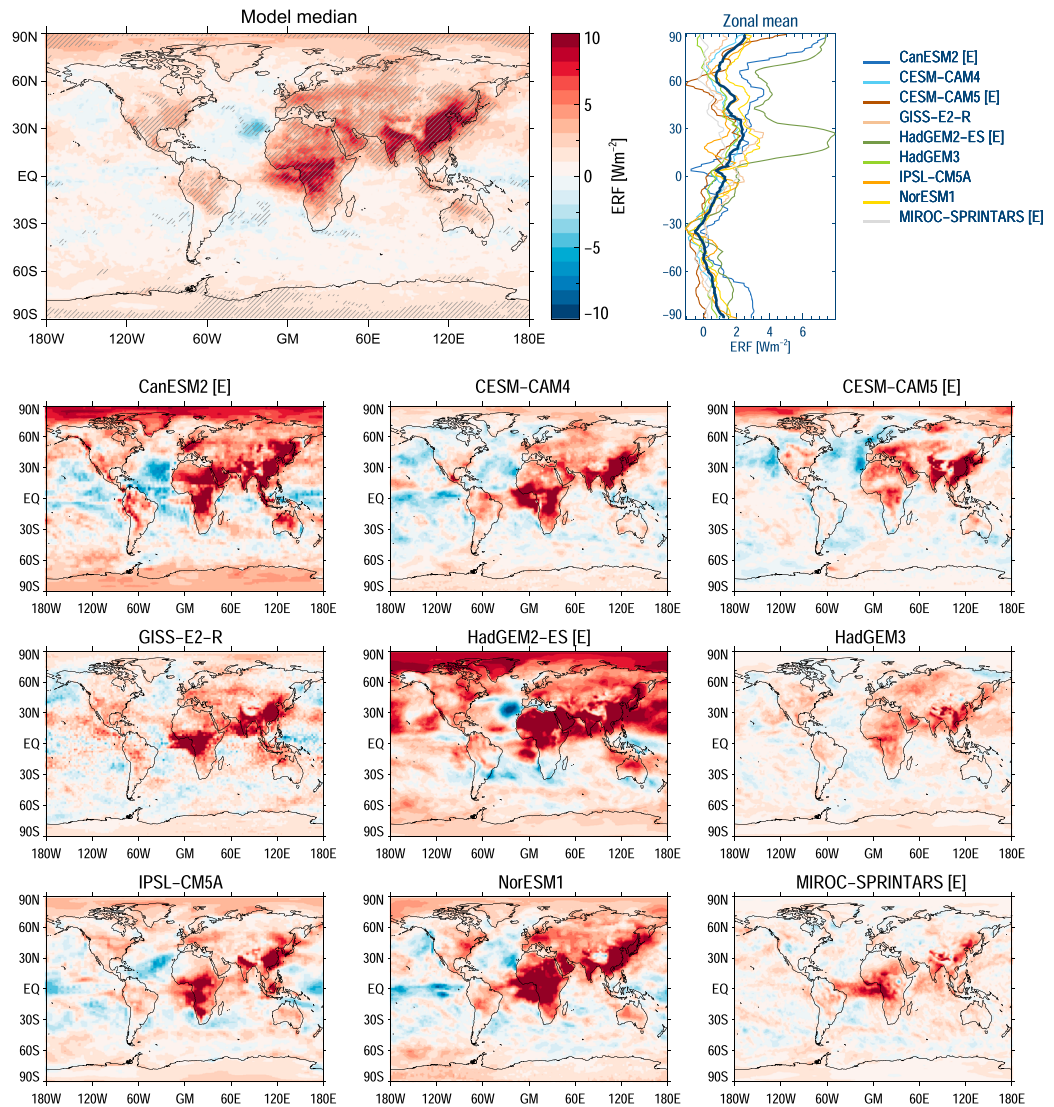


Figure 4. Annual mean model median ERF (top left) and zonally averaged temperature change for the model median (the black line) and individual models (top right). The remaining panels show individual model results. Data are based on the fixed-SST runs, and hatched areas in the model median map indicate grid cells for which values are more than one multimodel standard deviation away from zero.

temperature with altitude. Toward the top of the troposphere, this increase levels off and turns to a gradual reduction in warming with height, as the concentration of BC goes down. CanESM2 [E] has a very strong temperature increase up to about 100 hPa, at least partly due to its high increase in BC concentration (as seen in Figure S2, the global mean warming for CanESM2 [E] is only the fourth strongest when normalizing by BC burden change). Interestingly, IPSL-CM5A, for which the BC change in the lower atmosphere ($p > 500$ hPa) is weakest of all models, gives an above-average increase in temperature. It also has the strongest normalized warming of all models (Figure S2). As will be shown later, this is likely connected to a particularly strong cloud response. The temperature change in HadGEM2-ES [E] increases with height more than in any other model up to 250 hPa but decreases rapidly thereafter and even turns to a cooling at the highest levels—a temperature response more typical for a CO₂ increase, as shown in the model median panel below (dashed black line). A possible explanation is that the very high level of BC absorption of upwelling shortwave (SW) radiation in the troposphere strongly reduces the amount of SW available for absorption by ozone, which reduces the stratospheric heating and results in this case in a cooling relative to the base case. A pair of test runs performed by the HadGEM2-ES [E] model team where

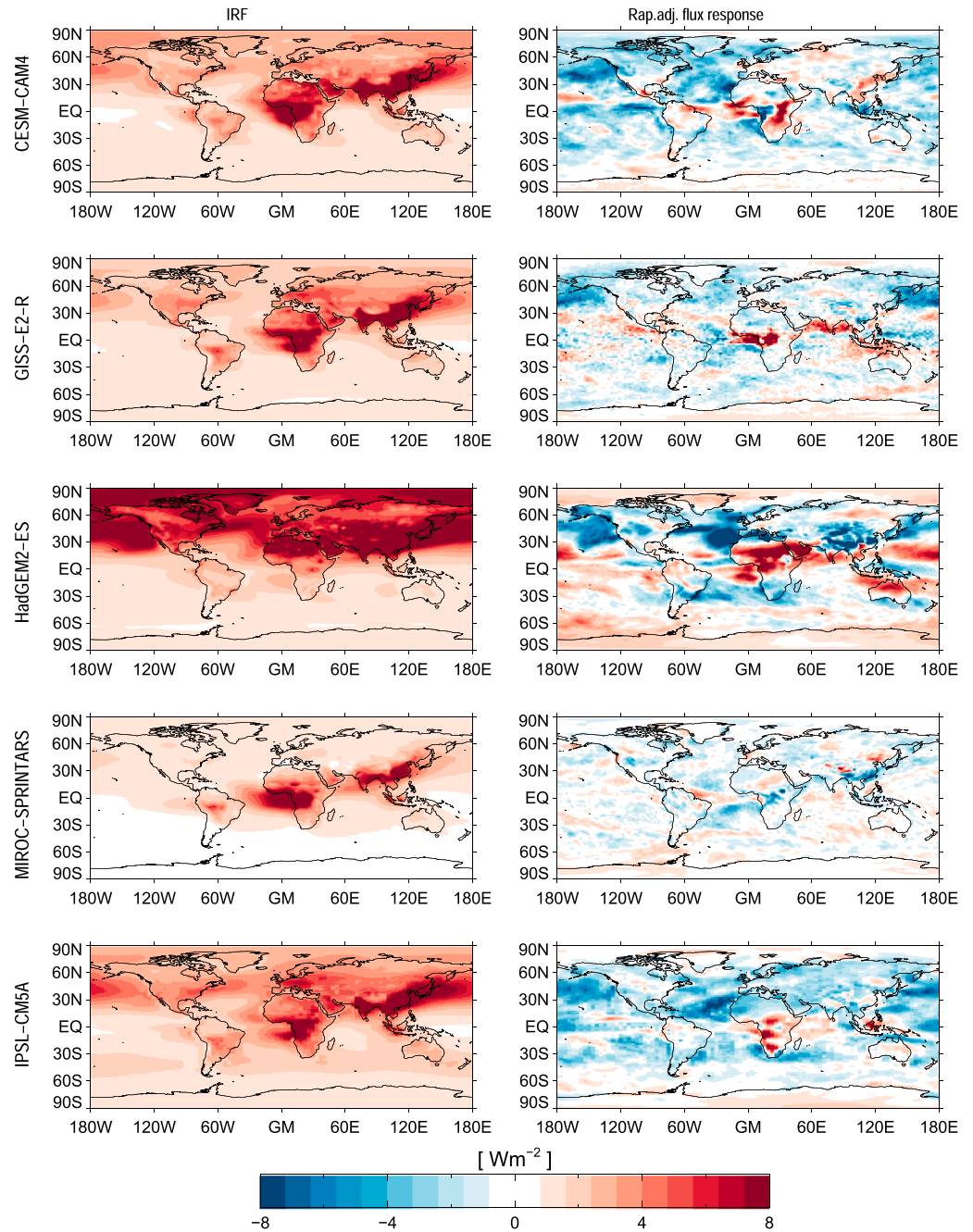


Figure 5. (left column) IRF and (right column) rapid adjustment flux response, based on double call simulations for five of the models.

the radiative effect of ozone was included and excluded, respectively, show that there is a (small) negative change in heating rate only if the radiative effect of ozone is included (see Figure S4). It is not known, however, whether this is the only cause of the BC-induced stratospheric cooling in HadGEM2-ES [E].

The increase in BC leads to an increase in the globally averaged amount of low clouds, but a reduction in middle- and high-level clouds. This is a cloud response typical to BC forcing, seen also in previous BC studies (e.g., Sand et al., 2015). Individual model numbers can be seen in Table S2, where low, midlevel, and high clouds are approximated as simple vertical averages of cloud fractions over given pressure intervals (1000–680 hPa, 680–440 hPa, and 440–50 hPa, respectively). The globally averaged cloud change profile is in general similar among the models (Figure 6), but HadGEM2-ES [E] produces increasing cloud amounts

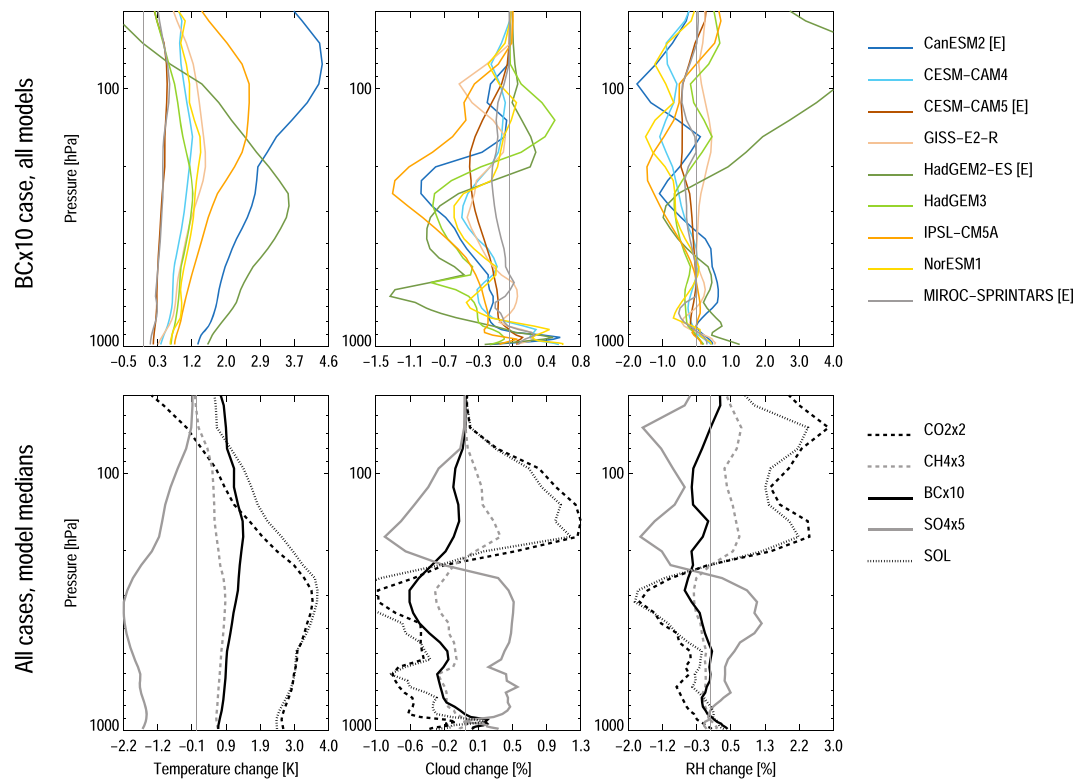


Figure 6. Globally averaged vertical profiles of change in (left column) temperature, (middle column) cloud amount, and (right column) relative humidity. The top row shows the change for the BCx10 case, for each of the models, while the bottom row shows the model median change for each of the five cases. Note different x axis limits between top and bottom panels. Profiles are based on the last 50 years of the coupled runs.

for altitudes above about 250 hPa, concurrent with a substantial increase in RH at the same levels, and HadGEM3 has reductions in cloud cover in all vertical layers below about 200 hPa. The total change in low and high cloud fractions is largest for IPSL-CM5A.

The total response in cloud fraction seen in Figure 6, with an increase at lower levels and a decrease at higher levels, is predominantly found over ocean regions, whereas over land, changes in cloud cover tend to have the same sign throughout the atmospheric column (Figure 7, top row). Most land regions have a reduction in low, midlevel, and high clouds, but in the regions with the strongest increases in BC, namely, India, East China, and the biomass burning regions of Central Africa, the cloud amount increases all through the atmospheric column. Changes in total cloud cover are generally largest over land, where the increase in lower tropospheric stability (LTS; calculated as the temperature difference between the 1,000 hPa and 780 hPa layers) is largest and where there is a reduction in sensible heat that is at least 5 times as strong as over ocean (not shown). Of the five experiments in the PDRMIP project, the BCx10 case induced the strongest changes in LTS, with a global decrease in 1,000 hPa – 780 hPa temperature difference of -0.16 K. Relative to the global temperature change, the number is -0.262 . For comparison, the corresponding numbers of LTS change per global temperature change for CO₂x2, CH₄x3, SO₄x5, and SOL are -0.012 , -0.015 , -0.039 , and -0.012 K, respectively.

As shown in Table 3, the model median total cloud change is -0.17% . The intermodel standard deviation is 0.34% —twice the median value. To investigate the reasons behind this large model spread, we have looked at how variables are connected in terms of Spearman’s rank correlation coefficients. Spatial correlations are calculated by correlating maps of time-averaged changes in, for example, total cloud fraction to maps of other changes or quantities for a given model. We also look at the “intermodel correlation” between pairs of globally averaged changes/values for the nine models, to check, for instance, if models with large changes in total cloud cover also have, for example, a high fraction of low clouds. For the latter correlations, changes are normalized by the global mean BC burden change for each model. We find that spatial correlations

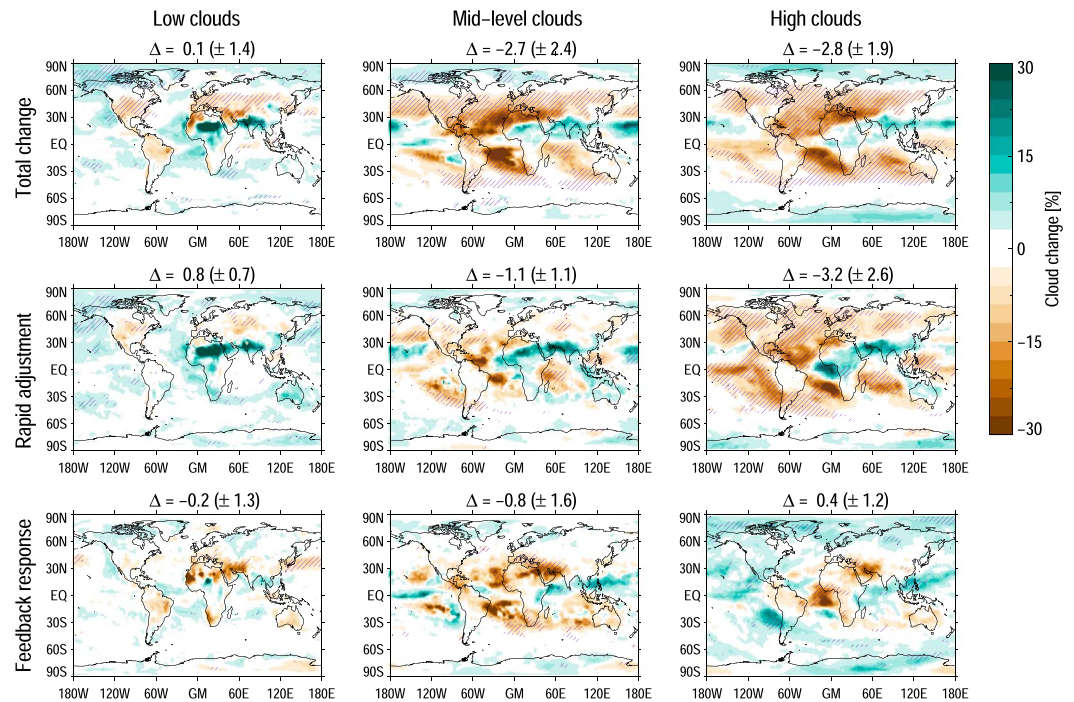


Figure 7. Model median (taken in each grid cell) changes in low cloud cover (approximated here as the simple vertical average in cloud cover for grid cells between the surface and up to 680 hPa), midlevel cloud cover (average between 680 and 440 hPa), and high cloud cover (average cloud cover above 440 hPa), given for the (top row) total response, the (middle row) rapid adjustment, and the (bottom row) feedback response, separately. Hatched areas in the model median map indicate grid cells for which values are more than one multimodel standard deviation away from zero. Globally averaged model median change and intermodel standard deviations are shown as numbers above each panel.

between the models' change in total cloud cover and the baseline cloud profile (as represented by the ratio of the average cloud fraction below to above 500 hPa) are around 0.4 and strongly significant for all models (see Table S3 for individual model correlation coefficients). This indicates that in regions where much of a model's clouds are located in the lower troposphere, the increase in clouds due to the BC perturbation is typically larger. The vertical distribution of clouds varies strongly between the models, as seen in Table 3 and Figure S5.

Previous studies have identified the fast response to dominate the total precipitation response to a BC perturbation (Andrews et al., 2010; Kvalevåg, Samset, & Myhre, 2013; Samset et al., 2016). Indeed, from the five models which provided calculations of IRF, we saw that the rapid adjustment flux response may

Table 3

The First Three Columns Are Calculated for the BASE Case, While the Others Reflect BCx10 – BASE Changes

	Low clouds (%)	Level for max low clouds (hPa)	BC ratio	Total cloud change (%)	Prec. change (mm/yr)
CanESM2 [E]	11.21	930	0.15	-0.26	-24.03
CESM-CAM4	14.22	867	0.32	+0.50	-18.77
CESM-CAM5 [E]	16.52	913	—	—	-13.19
GISS-E2-R	9.05	818	0.31	-0.81	-16.54
HadGEM2-ES [E]	12.16	861	—	-0.32	-21.12
HadGEM3	12.86	859	0.32	-0.59	+3.51
IPSL-CM5A	8.47	944	1.20	—	+0.16
NorESM1	14.47	857	0.30	+0.58	-15.07
MIROC-SPRINTARS [E]	8.65	876	0.32	-0.26	-14.95
Median (±SD)	12.16 (±2.86)	867 (±40)	0.32 (±0.35)	-0.17 (±0.34)	-15.07 (±9.19)

Note. Low clouds are here approximated as the simple vertical average (no overlap assumption) of the cloud fractions between 1,000 and 680 hPa levels. BC ratio refers to the ratio of the vertically averaged BC concentrations (given in mg m^{-3}) above 500 hPa to below 500 hPa, for the BASE case.

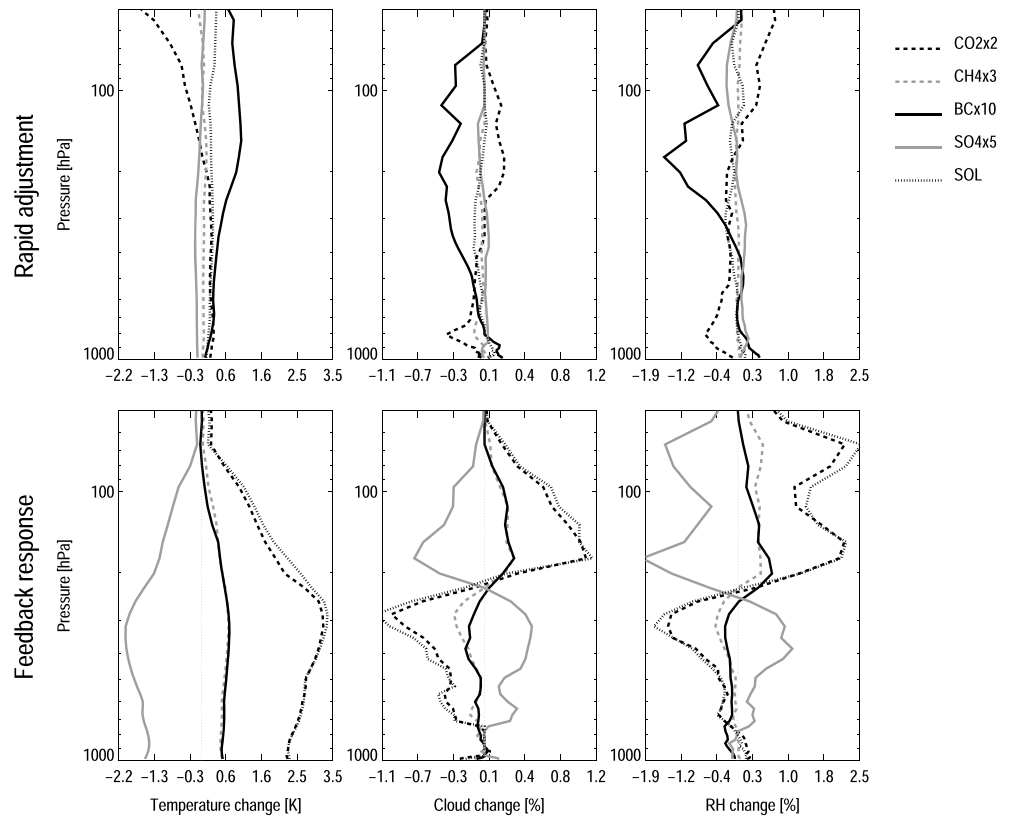


Figure 8. Multimodel median profiles of changes in temperature (K), cloud amount (%), and RH (%) for the five cases, separated into the (top row) fast response and the (bottom row) slow response.

constitute a significant part of the total ERF. Figure 8 is a version of the lower row of Figure 7, but showing the rapid adjustments (fSST, top row) and the feedback responses (coupled-fSST, bottom row) separately. Here we see that the BCx10 feedback response in temperature is more similar to the other drivers: increased instability in the upper troposphere leading to increased cloud cover. Concordant with the literature above, however, the rapid adjustments to increased BC (upper tropospheric stabilization and reduced cloud cover) dominate. In comparison, the CO₂x2 case has changes in the vertical distribution of clouds consistent with previous findings (Bony et al., 2013; Zelinka et al., 2014) and is dominated by the feedback response. Up to about 400 hPa, the rapid adjustments in temperature and cloud amounts are relatively similar between BCx10 and the other drivers. Above this level, the increase in BC induces an increase in upper tropospheric stability, giving rise to the reduction in cloud amount. For the other drivers, however, the upper troposphere becomes less stable and cloud amounts increase.

3.5. Precipitation Changes

In the BCx10 experiments, precipitation decreases globally in all models except HadGEM3 and IPSL-CM5A, with a median change of -15.1 (-24.0 to $+3.5$) mm/yr. Southern Hemisphere tropics and Northern Hemisphere midlatitudes experience the largest changes—see Figure 1. Note that even models with weak globally averaged precipitation change can have strong latitude-averaged precipitation signals. This demonstrates that although global responses to even such a highly exaggerated BC increase are small, there may still be substantial regional effects, as seen also in Figure 9. Previously reported BC precipitation responses such as a drying in the Mediterranean and an increase over the Indian Monsoon region (Kim et al., 2016) are robust features across the models, as are also the decrease in precipitation in the Amazon region and increased precipitation in north eastern Africa.

Samset et al. (2016) showed that for the BCx10 case, the rapid precipitation response was larger than the feedback response (the slow precipitation change) over oceans, contrary to the other climate drivers. Over

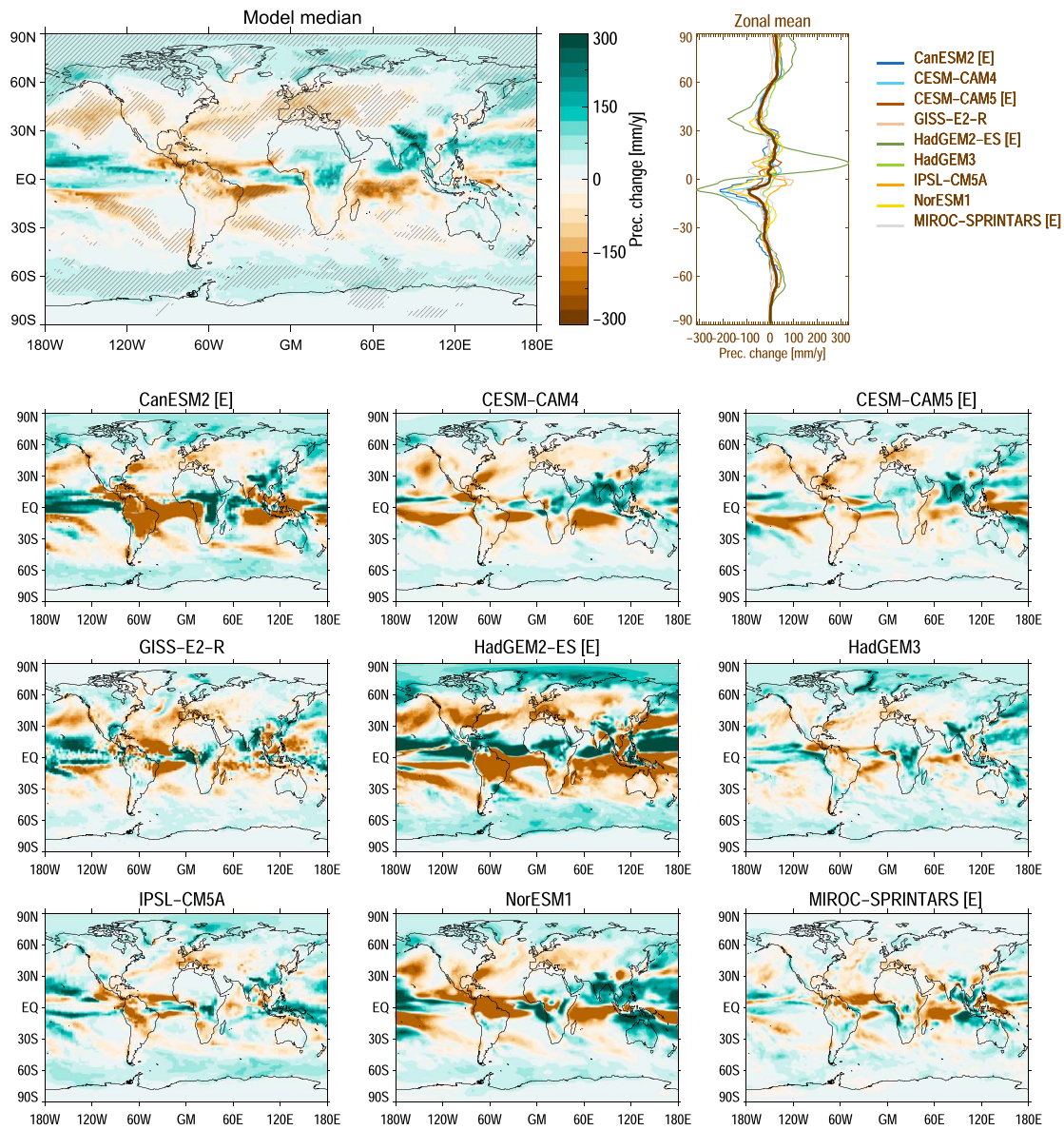


Figure 9. Annual mean model median change in precipitation (top left) and zonally averaged temperature change for the model median (the black line) and individual models (top right). The remaining panels show individual model results. Data are based on the last 50 years of the coupled runs, and hatched areas in the model median map indicate grid cells for which values are more than one multimodel standard deviation away from zero.

land, they showed that the precipitation response from BCx10 and CO₂x2 were dominated by the feedback response. Here we find that it is the convective (as opposed to the large-scale) precipitation component that dominates over oceans, which experience a large reduction in latent heat flux (not shown). The convective precipitation change is strongly negative, while over land it is weakly positive, yielding a globally averaged negative rapid response in precipitation.

As seen in Figure S2, the RSD for the BC burden change-normalized global precipitation change is 0.86 for precipitation—more than double the RSD for the temperature change. Understanding the main physical mechanisms behind the precipitation change might help us understand which model formulations differ the most, thus contributing to this large intermodel spread. Since we have seen that the convective precipitation component shows particularly large changes, it is relevant to investigate the role of changes in LTS. We find small and statistically insignificant spatial correlation between change in LTS and the rapid adjustment in precipitation (both total precipitation and convective) for all models. However, the total response (including

both rapid adjustment and feedback response) in convective precipitation has statistically significant spatial correlations to LTS for all models, with correlation coefficients averaging 0.39 for the emissions-based models and 0.26 for the concentration-driven models (see Table S3). How much a model's LTS changes will depend on the magnitude of the change in atmospheric absorption by BC and the subsequent atmospheric warming. Indeed, the inter-model correlation between changes in global mean atmospheric absorption and convective precipitation is -0.80 (for the rapid response; -0.72 for the total response) and significant on the 99% level. One factor contributing to the magnitude of the absorption is the mass absorption coefficient (MAC), which varies greatly between models. Table 1 gives MAC values for the models that were able to provide this and shows a range from 3.29 to 9.85 $\text{m}^2 \text{g}^{-1}$.

For some of the models, we also see a tendency that some of the rapid precipitation adjustment is influenced by the vertical distribution of BC. Spatial correlations between the rapid response in convective precipitation and the ratio of the average BC concentration below 500 hPa to the average above 500 hPa (the "BC ratio") has statistically significant correlations in the vicinity of -0.3 for several models (Table S3). This means that for some of the models, there is a tendency that regions where much of the BC is located at lower atmospheric levels (a high BC ratio) have smaller precipitation reductions.

Ongoing PDRMIP research indicates circulation changes (quantified as the dry static energy flux from land to ocean) to be the major contributor to the oceanic precipitation change in BCx10. We therefore also look at the spatial correlation between precipitation changes and changes in surface pressure. We find statistically significant spatial correlations between the total change in precipitation and change in surface pressure for all the models, with a model median correlation of -0.33 (varying between -0.30 for MIROC-SPRINTARS [E] and -0.42 for HadGEM2-ES [E]), signifying that some of the geographical variations in precipitation change can be attributed to changes in surface pressure.

4. Discussion

Previous PDRMIP studies as well as the present have confirmed earlier findings that BC-induced climate changes show a particularly large intermodel spread, even among the concentration-driven models. For instance, the intermodel relative standard deviation for the global mean temperature change is 28% for the CO₂x2 case and 86% for BCx10. In the PDRMIP BCx10 case, 4 of the 10 models (HadGEM2 [E], CanESM2 [E], CESM-CAM5 [E], and MIROC-SPRINTARS [E]) applied a tenfold increase in the baseline BC emissions instead of in the BC concentrations, causing differences in the absolute values of the BC concentration change. Samset et al. (2016) suggested in their PDRMIP study of fast and slow precipitation responses that the omission of any normalization with regards to changes in BC burden was likely a contributor to the observed model diversity, particularly due to the two different (emission-driven versus concentration-driven) model setups. Indeed, we find that the intermodel relative standard deviation of the global mean temperature change is reduced from 86% to 33% if we only consider models that used fixed concentrations, or to 40% if we look at BC burden-change-normalized temperature change.

For models with emission-driven setups, changes in, for example, atmospheric stability and resulting changes in precipitation release and wet removal will influence the BC concentrations, potentially with important feedback loops that may dampen or amplify the resulting change in BC. In a simulation study using the NorESM model, Sand et al. (2015) studied the climate response to BC perturbations, comparing the result of a 25-fold increase in BC concentrations to a 25-fold increase in BC emissions. In the concentration-driven simulations, the climate dynamics did not force the BC concentrations, while feedbacks between BC and other climate processes were allowed to operate in emission-driven simulations. They found that emission-driven climate responses were much larger than concentration-driven responses. In the present study we find that the total response (including both rapid adjustment and feedback response) in convective precipitation shows statistically significant spatial correlations to LTS for all models, but correlation coefficients are 50% higher for emissions-driven models than for concentration-driven models. In the emission-driven models, the reduced convective precipitation caused by the increased atmospheric stability leads to weakened wet removal, which increases BC concentrations and thus further increases in stability. Conceivably, this strengthens the relationship between LTS and convective precipitation in these models and may be one of the processes behind the differences found in Sand et al. (2015). Sand et al. (2015) (see also Booth & Bellouin, 2015) stress that one of the reasons for the large discrepancy between the emission-driven and

the concentration-driven simulation in their study may be the particularly efficient vertical transport in NorESM and that other models with less efficient transport may produce results with smaller differences. Allen and Landuyt (2014) compared convective mass fluxes and wet removal rates among several models, including HadGEM2-ES, CESM-CAM5, CanESM2, and MIROC5. They find that HadGEM2-ES has a relatively strong convective mass flux combined with the slowest wet removal rates of all the models investigated in that study, leading to prolonged lifetime of BC in the atmosphere. Indeed, Table 1 shows an estimated lifetime of 21.3 days for HadGEM2-ES [E]. CanESM2 [E] has relatively weak convection, but a slow wet removal rate enhances the potential BC impact by increasing the lifetime, and we here find a BC lifetime of 10.7 days. For CESM-CAM5 [E], on the other hand, previous studies (Liu et al., 2016) have documented that the model has too efficient removal rates, and Allen and Landuyt (2014) find wet removal rates for CAM5 to be the highest of all investigated models. This precludes long-range transport and lowers the lifetime of BC (estimated lifetime of 3.4 days; see Table 1) and therefore also the impact of a given BC perturbation on climate. Similarly, MIROC-SPRINTARS [E], with a slightly longer lifetime of 5.3 days, has an average wet deposition rate in Allen and Sherwood (2010), but a convective mass flux that is on the low side. Consequently, while the very strong climate responses HadGEM2-ES [E] and CanESM2 [E] can at least partly be a result of climate feedbacks on BC concentrations, CESM-CAM5 [E] and MIROC-SPRINTARS [E] have climate responses that are more similar to the concentration-driven models.

Aside from differences in the simulation setups, we have also looked into other potential causes of the large intermodel spread in the BC climate response. For some of the models, we find correlations between the rapid adjustment in convective precipitation and the vertical BC profile, represented by the BC ratio (coefficients are relatively small, -0.22 to -0.35 , but highly statistically significant). We also find significant correlations between each model's cloud response and the baseline cloud field. This means that at least for some models, differences in baseline vertical BC profiles or baseline cloud fields will contribute to the differences in the climate responses, as found in other studies (e.g., Johnson, 2005). In addition, the above mentioned spatial correlation between LTS and total change in normalized convective precipitation means that model differences in the efficiency of atmospheric warming may contribute to the magnitude of the precipitation response. A strong correlation between a model's change in atmospheric absorption and the change in convective precipitation underlines this.

Contributing to variations in model absorption are the individual MAC values. As presented in Table 1, these vary greatly between models, with values ranging from $3.29 \text{ m}^2 \text{ g}^{-1}$ (HadGEM2-ES [E]) to $9.85 \text{ m}^2 \text{ g}^{-1}$ (CESM-CAM5 [E]). Observations of MAC values demonstrate large spatial and seasonal variability, but typical values lie in the range of $8\text{--}12 \text{ m}^2 \text{ g}^{-1}$ (Bond & Bergstrom, 2006; Boucher et al., 2016; Zanatta et al., 2016). For instance, based on observations from rural sites in Europe, Zanatta et al. (2016) find a representative MAC value of $10.0 \text{ m}^2 \text{ g}^{-1}$.

In addition, the new and updated emission inventory Community Emissions Data System (CEDS) to be used in CMIP6 (Hoesly et al., 2017) has BC emissions around 75% higher than the CMIP5 emission data (Lamarque et al., 2010) used in this study. As seen in Myhre, Aas et al. (2017), globally averaged year 2000 emissions of BC are around 4.6 Tg yr^{-1} in CMIP5, but closer to 6.0 Tg yr^{-1} in the CEDS, which increase to around 8.0 Tg yr^{-1} in 2014. If both MAC values and present-day BC emissions in this study are on the low side, this implies that the climate response to the BC perturbations may be underestimated here. The combined low values of MAC in the models compared to more recent observations and higher estimates of BC emissions may indicate that the forcing and temperature response can be roughly a factor of 2 higher than presented here. On the other hand, the high modeled BC abundances in the upper troposphere compared to observation indicates a too long BC lifetime resulting in too strong forcing (Hodnebrog et al., 2014; Samset, Myhre, Herber, et al. (2014); Wang et al., 2014).

Efficacies of different climate forcers are compared in, for example, Hansen et al. (2005) and Yoshimori and Broccoli (2008). Hansen et al. (2005) calculate, using the GISS model, a fossil fuel BC efficacy of 0.78. This compares well with the GISS-E2-R efficacy of 0.86 in this paper. Yoshimori and Broccoli (2008) use the GFDL model and find a climate sensitivity of $0.46 \text{ K (W m}^{-2}\text{)}^{-1}$ for BC, comparable to our model median of 0.47 (± 0.33) $\text{K (W m}^{-2}\text{)}^{-1}$, and a BC efficacy of 0.58, which is lower than our model median of 0.80 (± 0.35). Note, however, that they define climate sensitivity as temperature change divided by IRF—not by ERF as we do. Both studies find the efficacy to vary strongly with regards to vertical BC distribution. The use of

ERF (as opposed to IRF) in the efficacy calculation in this study implies that the semidirect effect can constitute a substantial part of the model-to-model variation. Hence, each model's atmospheric absorption and original cloud fields will contribute to this variation (Stier et al., 2013). As stressed by Johnson (2005) in their investigation of semidirect effects using large eddy simulations, model estimates of aerosol forcing efficacy must be evaluated in the light of each model's skill in the evaluation of low-level clouds, as well as the sensitivity of these low cloud covers to aerosol heating. Notice, for instance, that IPSL-CM5A, which is the model with the lowest amount of low clouds, but concurrently the model with its maximum in low cloud fraction located the closest to the surface (Table 3 and Figure S5), has by far the largest BC efficacy.

As a final remark, we stress that the BC perturbation in these simulations is unrealistically high in the context of anthropogenic emissions. Since preindustrial times, emissions have increased from close to zero to about 4.5 Tg/yr (Lamarque et al., 2010). Results in the present study give climate responses to a perturbation 10 times larger. As discussed, for instance, in Fiedler, Stevens, and Mauritsen (2017), small ERF signals are difficult to detect when taking into account model-internal year-to-year variability. Given the nature of the BC impact on climate, where opposing effects are causing a weak total response, the exaggerated perturbations were therefore necessary in order to be able to study the climate impact with any significance. Ideally, the fully coupled simulations should be run for more than 100 years. Earlier tests with the models included in PDRMIP have shown that for the stronger CO₂x2 perturbation in the coupled ocean setup, 60–80% of the change to the final equilibrium state is reached after 100 years, while the final equilibration state requires several hundred additional simulation years to be reached (see, e.g., Samset et al., 2016). However, we are well within the regime where the additional response mainly scales with the surface temperature (Samset et al., 2016). Hence, while the present setup is influenced by the spread in forcing and response, that spread is heightened for BC due to the number of processes involved and the role of atmospheric shortwave absorption.

Extreme increases in atmospheric soot was the subject of investigation in several studies in the 1980s, where fires following a nuclear exchange was found to have the potential to cause so-called “nuclear winter” (Turco et al., 1983). As noted by Cess (1985), however, these extreme soot perturbations are so strong as to practically eliminate convective vertical mixing, which means that more moderate soot emissions where this mixing is merely dampened would cause “dramatically different” responses to the surface-atmosphere system. In the present study our strong perturbation in BC is still within the threshold for which the added BC warms climate and can be assumed to cause similar climate changes (only exaggerated) as the preindustrial to present-day increase. Our model median global warming of 0.67 (0.16 to 1.66) K following this perturbation would (assuming linearity) translate to a 1,850–2,000 warming of merely 0.07 K for emissions used in this work.

5. Conclusion

Earlier publications (Andrews et al., 2010; Kvalevåg et al., 2013) have shown that processes linked to atmospheric absorption, for which BC is a potent agent, are less consistently modeled than elements of climate change related to changes in surface temperature or TOA forcing. Therefore, BC stands out as a component that might cause significant model diversity in predictions of climate change. Through the Precipitation Driver Response Model Intercomparison Project (PDRMIP), climate responses to a tenfold increase in BC in nine global circulation models have been analyzed and compared to climate responses to four other climate drivers (CO₂, CH₄, the solar constant, and SO₄).

We find that the BCx10 case produces a global model median ERF of 0.82 W m⁻², with an intermodel spread of 0.41 to 2.91 W m⁻². Estimated instantaneous RF and the rapid adjustment from five of the models indicate that a relatively strong negative rapid adjustment balances some of the direct forcing, thus producing a smaller net ERF. The resulting change in surface temperature for a tenfold increase in BC is 0.67 (0.16 to 1.66) K. Translating the tenfold increase in BC to the present-day impact of anthropogenic BC would leave a warming of merely 0.07 K, but as noted above, present-day emissions are underestimated in here compared to recent studies so this number is probably higher.

Four of the nine models simulated the BC perturbations as a tenfold increase in anthropogenic emissions instead of an increase in concentrations, resulting in differences in the absolute value of the BC change. The intermodel spread in climate responses among the five models with consistent increases in BC

concentrations is substantially lower than the spread among all the models. Even so, the relative standard deviation of, for example, temperature change for this subset of models is 0.33 K globally. This indicates that the remaining role of model differences in baseline cloud fields or treatment of indirect effects or BC on snow, as well as the role of aerosol-specific features such as the mass absorption coefficient or the speed of BC aging or wet removal, is still significant.

Acknowledgments

All model results used for the present study are available to the public through the Norwegian NORSTORE data storage facility. For access, please see instructions at <http://www.cicero.uio.no/en/PDRMIP/PDRMIP-data-access>. PDRMIP is partly funded through the Norwegian Research Council project NAPEX (project 229778). T. Takemura was supported by the supercomputer system of the National Institute for Environmental Studies, Japan; the Environment Research and Technology Development Fund (S-12-3) of the Ministry of the Environment, Japan; and JSPS KAKENHI grants 15H01728 and 15K12190. D. Olivie, A. Kirkevåg, and T. Iversen were supported by the Norwegian Research Council through the projects EVA (grant 229771), EarthClim (207711/E10), NOTUR (nn2345k), and NorStore (ns2345k). M. Kasoar and A. Voulgarakis are supported by the Natural Environment Research Council under grant NE/K500872/1. Simulations with HadGEM3-GA4 were performed using the MONSOON system, a collaborative facility supplied under the Joint Weather and Climate Research Programme, which is a strategic partnership between the Met Office and the Natural Environment Research Council. We acknowledge the NASA High-End Computing Program through the NASA Center for Climate Simulation at Goddard Space Flight Center for computational resources to run the GISS-E2R model. Olivier Boucher acknowledges HPC resources from TGCC under the gencmip6 allocation provided by GENCI (Grand Equipement National de Calcul Intensif). T. R. and P. F. were supported by NERC grants NE/K007483/1 and NE/N006038/1.

References

- Ackerman, A. S., Toon, O. B., Stevens, D. E., Heymsfield, A. J., Ramanathan, V., & Welton, E. J. (2000). Reduction of tropical cloudiness by soot. *Science*, *288*(5468), 1042–1047. <https://doi.org/10.1126/science.288.5468.1042>
- Allen, R. J., & Landuyt, W. (2014). The vertical distribution of black carbon in CMIP5 models: Comparison to observations and the importance of convective transport. *Journal of Geophysical Research: Atmospheres*, *119*, 4808–4835. <https://doi.org/10.1002/2014JD021595>
- Allen, R. J., & Sherwood, S. C. (2010). Aerosol-cloud semi-direct effect and land-sea temperature contrast in a GCM. *Geophysical Research Letters*, *37*, L07702. <https://doi.org/10.1029/2010GL042759>
- Andrews, T., Forster, P. M., Boucher, O., Bellouin, N., & Jones, A. (2010). Precipitation, radiative forcing and global temperature change. *Geophysical Research Letters*, *37*, L14701. <https://doi.org/10.1029/2010GL043991>
- Baker, L. H., Collins, W. J., Olivie, D. J. L., Cherian, R., Hodnebrog, Ø., Myhre, G., & Quaas, J. (2015). Climate responses to anthropogenic emissions of short-lived climate pollutants. *Atmospheric Chemistry and Physics*, *15*(14), 8201–8216. <https://doi.org/10.5194/acp-15-8201-2015>
- Bond, T. C., & Bergstrom, R. W. (2006). Light absorption by carbonaceous particles: An investigative review. *Aerosol Science and Technology*, *40*(1), 27–67. <https://doi.org/10.1080/02786820500421521>
- Bond, T. C., Doherty, S. J., Fahey, D. W., Forster, P. M., Bernsten, T., DeAngelo, B. J., ... Zender, C. S. (2013). Bounding the role of black carbon in the climate system: A scientific assessment. *Journal of Geophysical Research: Atmospheres*, *118*, 5380–5552. <https://doi.org/10.1002/jgrd.50171>
- Bony, S., Bellon, G., Kloke, D., Sherwood, S., Fermepein, S., & Denvil, S. (2013). Robust direct effect of carbon dioxide on tropical circulation and regional precipitation. *Nature Geoscience*, *6*(6), 447–451. <https://doi.org/10.1038/ngeo1799>
- Booth, B., & Bellouin, N. (2015). Climate change: Black carbon and atmospheric feedbacks. *Nature*, *519*(7542), 167–168. <https://doi.org/10.1038/519167a>
- Boucher, O., Balkanski, Y., Hodnebrog, Ø., Myhre, C. L., Myhre, G., Quaas, J., ... Wang, R. (2016). Jury is still out on the radiative forcing by black carbon. *Proceedings of the National Academy of Sciences*, *113*(35), E5092–E5093. <https://doi.org/10.1073/pnas.1607005113>
- Boucher, O., Randall, D., Artaxo, P., Bretherton, C., Feingold, G., Forster, P., ... Zhang, X. Y. (2013). Clouds and aerosols. In T. F. Stocker, et al. (Eds.), *Climate Change 2013: The Physical Science Basis. Contribution of Working Group I to the Fifth Assessment Report of the Intergovernmental Panel on Climate Change* (pp. 571–658). Cambridge, UK and New York: Cambridge University Press. <https://doi.org/10.1017/CBO9781107415324.016>
- Cess, R. D. (1985). Nuclear war: Illustrative effects of atmospheric smoke and dust upon solar radiation. *Climatic Change*, *7*(2), 237–251. <https://doi.org/10.1007/bf00140508>
- Chen, Y., & Penner, J. E. (2005). Uncertainty analysis for estimates of the first indirect aerosol effect. *Atmospheric Chemistry and Physics*, *5*(11), 2935–2948. <https://doi.org/10.5194/acp-5-2935-2005>
- Cohen, J. B., & Wang, C. (2014). Estimating global black carbon emissions using a top-down Kalman filter approach. *Journal of Geophysical Research: Atmospheres*, *119*, 307–323. <https://doi.org/10.1002/2013JD019912>
- Fiedler, S., Stevens, B., & Mauritsen, T. (2017). On the sensitivity of anthropogenic aerosol forcing to model-internal variability and parameterizing a Twomey effect. *Journal of Advances in Modeling Earth Systems*, *9*(2), 1325–1341. <https://doi.org/10.1002/2017MS000932>
- Forster, P. M., Richardson, T., Maycock, A. C., Smith, C. J., Samset, B. H., Myhre, G., ... Schulz, M. (2016). Recommendations for diagnosing effective radiative forcing from climate models for CMIP6. *Journal of Geophysical Research: Atmospheres*, *121*, 12,460–12,475. <https://doi.org/10.1002/2016JD025320>
- Ghan, S. J., Liu, X., Easter, R. C., Zaveri, R., Rasch, P. J., Yoon, J.-H., & Eaton, B. (2012). Toward a minimal representation of aerosols in climate models: Comparative decomposition of aerosol direct, Semidirect, and indirect radiative forcing. *Journal of Climate*, *25*(19), 6461–6476. <https://doi.org/10.1175/jcli-d-11-00650.1>
- Gustafsson, Ö., & Ramanathan, V. (2016). Convergence on climate warming by black carbon aerosols. *Proceedings of the National Academy of Sciences*, *113*(16), 4243–4245. <https://doi.org/10.1073/pnas.1603570113>
- Hansen, J., Sato, M., Ruedy, R., Nazarenko, L., Lacis, A., Schmidt, G. A., ... Zhang, S. (2005). Efficacy of climate forcings. *Journal of Geophysical Research*, *110*, D18104. <https://doi.org/10.1029/2005JD005776>
- Hodnebrog, Ø., Myhre, G., & Samset, B. H. (2014). How shorter black carbon lifetime alters its climate effect. *Nature Communications*, *5*, 5065. <https://doi.org/10.1038/ncomms6065>
- Hoesly, R. M., Smith, S. J., Feng, L., Klimont, Z., Janssens-Maenhout, G., Pitkanen, T., ... Zhang, Q. (2017). Historical (1750–2014) anthropogenic emissions of reactive gases and aerosols from the Community Emission Data System (CEDS). *Geoscientific Model Development Discussion*, *2017*, 1–41. <https://doi.org/10.5194/gmd-2017-43>
- Jacobson, M. Z. (2010). Short-term effects of controlling fossil-fuel soot, biofuel soot and gases, and methane on climate, Arctic ice, and air pollution health. *Journal of Geophysical Research*, *115*, D14209. <https://doi.org/10.1029/2009JD013795>
- Janssens-Maenhout, G., Crippa, M., Guizzardi, D., Dentener, F., Muntean, M., Pouliot, G., ... Li, M. (2015). HTAP_v2.2: A mosaic of regional and global emission grid maps for 2008 and 2010 to study hemispheric transport of air pollution. *Atmospheric Chemistry and Physics*, *15*(19), 11,411–11,432. <https://doi.org/10.5194/acp-15-11411-2015>
- Johnson, B. T. (2005). The semidirect aerosol effect: Comparison of a single-column model with large eddy simulation for marine stratocumulus. *Journal of Climate*, *18*(1), 119–130. <https://doi.org/10.1175/jcli-3233.1>
- Jones, A., Haywood, J. M., & Boucher, O. (2007). Aerosol forcing, climate response and climate sensitivity in the Hadley Centre climate model. *Journal of Geophysical Research*, *112*, D20211. <https://doi.org/10.1029/2007JD008688>
- Kim, M.-K., Lau, W. K. M., Kim, K.-M., Sang, J., Kim, Y.-H., & Lee, W.-S. (2016). Amplification of ENSO effects on Indian summer monsoon by absorbing aerosols. *Climate Dynamics*, *46*(7–8), 2657–2671. <https://doi.org/10.1007/s00382-015-2722-y>
- Koch, D., & Del Genio, A. D. (2010). Black carbon semi-direct effects on cloud cover: Review and synthesis. *Atmospheric Chemistry and Physics*, *10*(16), 7685–7696. <https://doi.org/10.5194/acp-10-7685-2010>

- Kovilakam, M., & Mahajan, S. (2016). Confronting the "Indian summer monsoon response to black carbon aerosol" with the uncertainty in its radiative forcing and beyond. *Journal of Geophysical Research: Atmospheres*, *121*, 7833–7852. <https://doi.org/10.1002/2016JD024866>
- Kvalevåg, M. M., Samset, B. H., & Myhre, G. (2013). Hydrological sensitivity to greenhouse gases and aerosols in a global climate model. *Geophysical Research Letters*, *40*(7), 1432–1438. <https://doi.org/10.1002/grl.50318>
- Lamarque, J. F., Bond, T. C., Eyring, V., Granier, C., Heil, A., Klimont, Z., ... Vuuren, D. P. (2010). Historical (1850–2000) gridded anthropogenic and biomass burning emissions of reactive gases and aerosols: Methodology and application. *Atmospheric Chemistry and Physics*, *10*(15), 7017–7039. <https://doi.org/10.5194/acp-10-7017-2010>
- Liu, J., Scheuer, E., Dibb, J., Ziemba, L. D., Thornhill, K. L., Anderson, B. E., ... Weber, R. J. (2014). Brown carbon in the continental troposphere. *Geophysical Research Letters*, *41*, 2191–2195. <https://doi.org/10.1002/2013GL058976>
- Liu, X., Ma, P. L., Wang, H., Tilmes, S., Singh, B., Easter, R. C., ... Rasch, P. J. (2016). Description and evaluation of a new four-mode version of the Modal Aerosol Module (MAM4) within version 5.3 of the Community Atmosphere Model. *Geoscientific Model Development*, *9*(2), 505–522. <https://doi.org/10.5194/gmd-9-505-2016>
- Lohmann, U., & Feichter, J. (2005). Global indirect aerosol effects: A review. *Atmospheric Chemistry and Physics*, *5*(3), 715–737. <https://doi.org/10.5194/acp-5-715-2005>
- Mahajan, S., Evans, K. J., Hack, J. J., & Truesdale, J. E. (2013). Linearity of climate response to increases in black carbon aerosols. *Journal of Climate*, *26*(20), 8223–8237. <https://doi.org/10.1175/jcli-d-12-00715.1>
- Mahmood, R., von Salzen, K., Flanner, M., Sand, M., Langner, J., Wang, H., & Huang, L. (2016). Seasonality of global and Arctic black carbon processes in the Arctic Monitoring and Assessment Programme models. *Journal of Geophysical Research: Atmospheres*, *121*, 7100–7116. <https://doi.org/10.1002/2016JD024849>
- Myhre, G., Aas, W., Cherian, R., Collins, W., Faluvegi, G., Flanner, M., ... Tsyro, S. (2017). Multi-model simulations of aerosol and ozone radiative forcing due to anthropogenic emission changes during the period 1990–2015. *Atmospheric Chemistry and Physics*, *17*(4), 2709–2720. <https://doi.org/10.5194/acp-17-2709-2017>
- Myhre, G., Forster, P. M., Samset, B. H., Hodnebrog, Ø., Sillmann, J., Aalberg, S. G., ... Zwiers, F. (2017). PDRMIP: A Precipitation Driver and Response Model Intercomparison Project. Protocol and preliminary results. *Bulletin of the American Meteorological Society*, *98*(6), 1185–1198. <https://doi.org/10.1175/BAMS-D-16-0019.1>
- Myhre, G., & Samset, B. H. (2015). Standard climate models radiation codes underestimate black carbon radiative forcing. *Atmospheric Chemistry and Physics*, *15*(5), 2883–2888. <https://doi.org/10.5194/acp-15-2883-2015>
- Myhre, G., Samset, B. H., Schulz, M., Balkanski, Y., Bauer, S., Bernsten, T. K., ... Zhou, C. (2013). Radiative forcing of the direct aerosol effect from AeroCom Phase II simulations. *Atmospheric Chemistry and Physics*, *13*(4), 1853–1877. <https://doi.org/10.5194/acp-13-1853-2013>
- Peng, J., Hu, M., Guo, S., Du, Z., Zheng, J., Shang, D., ... Zhang, R. (2016). Markedly enhanced absorption and direct radiative forcing of black carbon under polluted urban environments. *Proceedings of the National Academy of Sciences*, *113*(16), 4266–4271. <https://doi.org/10.1073/pnas.1602310113>
- Samset, B. H., & Myhre, G. (2015). Climate response to externally mixed black carbon as a function of altitude. *Journal of Geophysical Research: Atmospheres*, *120*, 2913–2927. <https://doi.org/10.1002/2014JD022849>
- Samset, B. H., Myhre, G., Forster, P. M., Hodnebrog, Ø., Andrews, T., Faluvegi, G., ... Voulgarakis, A. (2016). Fast and slow precipitation responses to individual climate forcings: A PDRMIP multimodel study. *Geophysical Research Letters*, *43*, 2782–2791. <https://doi.org/10.1002/2016GL068064>
- Samset, B. H., Myhre, G., Herber, A., Kondo, Y., Li, S.-M., Moteki, N., ... Zhang, K. (2014). Modelled black carbon radiative forcing and atmospheric lifetime in AeroCom Phase II constrained by aircraft observations. *Atmospheric Chemistry and Physics*, *14*(22), 12465–12477. <https://doi.org/10.5194/acp-14-12465-2014>
- Samset, B. H., Myhre, G., & Schulz, M. (2014). Upward adjustment needed for aerosol radiative forcing uncertainty. *Nature Climate Change*, *4*(4), 230–232. <https://doi.org/10.1038/nclimate2170>
- Samset, B. H., Myhre, G., Schulz, M., Balkanski, Y., Bauer, S., Bernsten, T. K., ... Zhang, K. (2013). Black carbon vertical profiles strongly affect its radiative forcing uncertainty. *Atmospheric Chemistry and Physics*, *13*(5), 2423–2434. <https://doi.org/10.5194/acp-13-2423-2013>
- Sand, M., Bernsten, T. K., Kay, J. E., Lamarque, J. F., Seland, Ø., & Kirkevåg, A. (2013). The Arctic response to remote and local forcing of black carbon. *Atmospheric Chemistry and Physics*, *13*(1), 211–224. <https://doi.org/10.5194/acp-13-211-2013>
- Sand, M., Bernsten, T. K., Seland, Ø., & Kristjánsson, J. E. (2013). Arctic surface temperature change to emissions of black carbon within Arctic or midlatitudes. *Journal of Geophysical Research: Atmospheres*, *118*, 7788–7798. <https://doi.org/10.1002/jgrd.50613>
- Sand, M., Iversen, T., Bohlinger, P., Kirkevåg, A., Seierstad, I., Seland, Ø., & Sorteberg, A. (2015). A standardized global climate model study showing unique properties for the climate response to black carbon aerosols. *Journal of Climate*, *28*(6), 2512–2526. <https://doi.org/10.1175/jcli-d-14-00050.1>
- Schwarz, J. P., Samset, B. H., Perring, A. E., Spackman, J. R., Gao, R. S., Stier, P., ... Fahey, D. W. (2013). Global-scale seasonally resolved black carbon vertical profiles over the Pacific. *Geophysical Research Letters*, *40*, 5542–5547. <https://doi.org/10.1002/2013GL057775>
- Sherwood, S. C., Bony, S., Boucher, O., Bretherton, C., Forster, P. M., Gregory, J. M., & Stevens, B. (2015). Adjustments in the forcing-feedback framework for understanding climate change. *Bulletin of the American Meteorological Society*, *96*(2), 217–228. <https://doi.org/10.1175/bams-d-13-00167.1>
- Shindell, D., & Faluvegi, G. (2009). Climate response to regional radiative forcing during the twentieth century. *Nature Geoscience*, *2*(4), 294–300. <https://doi.org/10.1038/ngeo473>
- Stanhill, G., & Cohen, S. (2001). Global dimming: A review of the evidence for a widespread and significant reduction in global radiation with discussion of its probable causes and possible agricultural consequences. *Agricultural and Forest Meteorology*, *107*(4), 255–278. [https://doi.org/10.1016/S0168-1923\(00\)00241-0](https://doi.org/10.1016/S0168-1923(00)00241-0)
- Stier, P., AJ Schutgens, N., Bellouin, N., Bian, H., Boucher, O., Chin, M., ... Zhou, C. (2013). Host model uncertainties in aerosol radiative forcing estimates: Results from the AeroCom prescribed intercomparison study. *Atmospheric Chemistry and Physics*, *13*(6), 3245–3270. <https://doi.org/10.5194/acp-13-3245-2013>
- Stohl, A., Klimont, Z., Eckhardt, S., Kupiainen, K., Shevchenko, V. P., Kopeikin, V. M., & Novigatsky, A. N. (2013). Black carbon in the Arctic: The underestimated role of gas flaring and residential combustion emissions. *Atmospheric Chemistry and Physics*, *13*(17), 8833–8855. <https://doi.org/10.5194/acp-13-8833-2013>
- Takemura, T., Egashira, M., Matsuzawa, K., Ichijo, H., Oishi, R., & Abe-Ouchi, A. (2009). A simulation of the global distribution and radiative forcing of soil dust aerosols at the Last Glacial Maximum. *Atmospheric Chemistry and Physics*, *9*(9), 3061–3073. <https://doi.org/10.5194/acp-9-3061-2009>
- Takemura, T., Nozawa, T., Emori, S., Nakajima, T. Y., & Nakajima, T. (2005). Simulation of climate response to aerosol direct and indirect effects with aerosol transport-radiation model. *Journal of Geophysical Research*, *110*, L18815. <https://doi.org/10.1029/2004JD005029>

- Turco, R. P., Toon, O. B., Ackerman, T. P., Pollack, J. B., & Sagan, C. (1983). Nuclear winter: Global consequences of Multiple nuclear explosions. *Science*, 222(4630), 1283–1292. <https://doi.org/10.1126/science.222.4630.1283>
- Twomey, S. (1974). Pollution and the planetary albedo. *Atmospheric Environment*, 8(12), 1251–1256. [https://doi.org/10.1016/0004-6981\(74\)90004-3](https://doi.org/10.1016/0004-6981(74)90004-3)
- Wang, Q., Jacob, D. J., Spackman, J. R., Perring, A. E., Schwarz, J. P., Moteki, N., ... Barrett, S. R. H. (2014). Global budget and radiative forcing of black carbon aerosol: Constraints from pole-to-pole (HIPPO) observations across the Pacific. *Journal of Geophysical Research: Atmospheres*, 119, 195–206. <https://doi.org/10.1002/2013JD020824>
- Yoshimori, M., & Broccoli, A. J. (2008). Equilibrium response of an atmosphere–mixed Layer Ocean model to different radiative forcing agents: Global and zonal mean response. *Journal of Climate*, 21(17), 4399–4423. <https://doi.org/10.1175/2008jcli2172.1>
- Zanatta, M., Gysel, M., Bukowiecki, N., Müller, T., Weingartner, E., Areskoug, H., ... Laj, P. (2016). A European aerosol phenomenology-5: Climatology of black carbon optical properties at 9 regional background sites across Europe. *Atmospheric Environment*, 145, 346–364. <https://doi.org/10.1016/j.atmosenv.2016.09.035>
- Zelinka, M. D., Andrews, T., Forster, P. M., & Taylor, K. E. (2014). Quantifying components of aerosol-cloud-radiation interactions in climate models. *Journal of Geophysical Research: Atmospheres*, 119, 7599–7615. <https://doi.org/10.1002/2014JD021710>
- Zhuang, B., Liu, Q., Wang, T., Yin, C., Li, S., Xie, M., ... Mao, H. (2013). Investigation on semi-direct and indirect climate effects of fossil fuel black carbon aerosol over China. *Theoretical and Applied Climatology*, 114(3-4), 651–672. <https://doi.org/10.1007/s00704-013-0862-8>